Available online at www.sciencedirect.com
ScienceDirect
Journal of Nuclear Materials 361 (2007) 289–297
journal of nuclear materials
www.elsevier.com/locate/jnucmat

Monte Carlo simulations of stray neutron radiation exposures in proton therapy

Yuanshui Zheng *, Wayne Newhauser, Jonas Fontenot, Nicholas Koch, Radhe Mohan

Department of Radiation Physics, Unit 94, The University of Texas, MD Anderson Cancer Center, 1515 Holcombe Boulevard, Houston, TX 77030, USA

Abstract

Proton radiotherapy patients receive unwanted stray neutron radiation generated in the treatment apparatus. The literature on this neutron radiation is sparse and disparate and pertains mainly to unique or antiquated systems. The present work reports on neutron dose equivalent per therapeutic absorbed dose (H/D) in a contemporary proton therapy system. We applied the Monte Carlo method to predict neutron exposure as a function of treatment field size and location in the treatment room. For a 250-MeV proton beam, H/D values at isocenter increased from 13 to 20 mSv Gy^{-1} as the collimating aperture was decreased from 18×18 to 0×0 cm^2. H/D values generally decreased with distance from isocenter (20 mSv Gy^{-1} at isocenter versus 0.9 mSv Gy^{-1} at a distance of 150 cm). Neutron spectral fluence calculations revealed that >50% of the dose equivalent at all locations considered was from neutrons >10 MeV.

PACS: 87.56.−v; 87.50.−a; 87.53.Pb,Qc

1. Introduction

Radiation therapy is a widely used cancer treatment option. Interest in proton radiation therapy has been increasing in recent years because it offers superior normal tissue sparing when compared to conventional photon radiation therapy. Accelerated proton beams are modified so that they provide uniform doses to tumors that have very different shapes, sizes, and locations in the body. Passive beam-spreading techniques [1–3] are employed at the majority of the 25 proton therapy centers currently in operation worldwide [4]. Passive beam spreading typically uses a rotating range-modulator wheel to provide a uniform proton dose to the tumor in depth, static scattering foils to spread and flatten the beam laterally, and a final collimating aperture to conform the beam's cross-sectional area to the tumor. As protons of up to 250 MeV interact in collimators and other beamline components, copious quantities of neutrons are produced, leading to unwanted whole-body neutron exposures to the patients.

The literature on secondary neutron exposures to proton therapy patients is sparse, and quantitative results are disparate. Qualitatively, however, the literature is in general agreement that secondary

* Corresponding author. Tel.: +1 713 745 2172; fax: +1 713 563 2479.
E-mail address: yszheng@mdanderson.org (Y. Zheng).

0022-3115/$ - see front matter
doi:10.1016/j.jnucmat.2006.12.016

neutron doses from proton therapy are small but not negligible. Binns and Hough [5] reported measured neutron dose equivalent per therapeutic absorbed dose (H/D) values between 33 and 80 mSv Gy^{-1} in the 200-MeV passively scattered beamline of the National Accelerator Centre (NAC) at lateral distances ranging from 30 to 120 cm from the beam axis. Agosteo et al. [6] used Monte Carlo models of several passively scattered proton therapy systems (at the NAC, Centre Antoine-Lacassagne, and Paul Scherrer Institute) to estimate a maximum neutron absorbed dose per therapeutic dose of up to 10 mGy Gy^{-1} for a deep-tumor treatment. Yan et al. [7] measured the H/D values in the Harvard Cyclotron Laboratory's 160-MeV proton treatment beamlines, which included a large-field nozzle, a radiosurgery nozzle, and an ocular nozzle. They reported H/D values for the large-field nozzle ranging from 0.91 to 15 mSv Gy^{-1} for increasing angles around the treatment nozzle at a distance of 50 cm from the isocenter. Polf and Newhauser [8,9] subsequently confirmed the Harvard large-field nozzle measurements with Monte Carlo simulations, reporting H/D values of up to 10 mSv Gy^{-1} around the treatment nozzle for a beam with a spread-out Bragg peak (SOBP) width of 8.5 cm. Similarly, Fontenot et al. [10] confirmed the H/D values measured in the Harvard radiosurgery beamline [7], also using Monte Carlo methods. Schneider et al. [11] reported an H/D value for a spot scanning system at the Paul Scherrer Institute of approximately 4 mSv Gy^{-1} for large target volumes by performing both measurements and Monte Carlo simulations. Roy and Sandison [12] measured fetal H/D values of about 0.20 mSv Gy^{-1} for a 200-MeV proton field delivered to the mother's chest at the Indiana University Cyclotron Facility. Jiang et al. [13] reported Monte Carlo predictions of whole-body effective doses of 2.3 mSv Gy^{-1} and 0.6 mSv Gy^{-1} for proton plans of lung and paranasal sinus treatments, respectively. We attribute the large differences in previously published H/D values to differences in the beam delivery systems and experimental conditions (e.g., field sizes) and large uncertainties in the measurements and simulations. Because the cross-sectional area of proton therapy fields varies between a few square centimeters and >600 cm^2, the influence of the collimated field size is thought to be key in quantifying H/D values. However, to our knowledge, a systematic study of the influence of field size on H/D values has not been reported.

The aim of this work was to estimate the neutron dose equivalent per therapeutic absorbed dose, H/D, which would be delivered to patients treated at a recently commissioned proton therapy facility using a state-of-the-art passive beam delivery system. In particular, we studied the variation in H/D with proton field size, as determined by the final beam-limiting collimator, and with location in the treatment room. Monte Carlo methods were used to estimate the neutron dose equivalent, H, caused by neutrons produced in the beam delivery system; the therapeutic absorbed dose, D; and the distribution of dose equivalent in neutron energy, $H(E)$.

2. Methods and materials

2.1. Modeling of the beam delivery apparatus

We used the MCNPX Monte Carlo radiation transport code (version 2.5e) [14] to simulate the proton therapy beam delivery system because it has been extensively benchmarked against measurements in proton therapy applications [8–10,15]. MCNPX is a general-purpose code that can track up to 34 particle types, including protons. Nuclear interaction mechanisms modeled included elastic scattering, intranuclear cascades, and pre-equilibrium and evaporation emissions. For energies from 1 keV to 150 MeV, evaluated nuclear interaction cross-section libraries were used [16]; above this energy, hadronic cross-sections were estimated using the Bertini intranuclear-cascade model [17] for nucleons and pions and the ISABEL model [18] for other particle types. The cutoff energy for proton transport was 1 MeV. In a previous study, a special code system was developed to automatically generate MCNPX input files that model the proton treatment nozzles based on the mechanical design data for each component [19,20].

We simulated the passive scattering beam delivery system used at our institution (Hitachi America, Ltd., Brisbane, CA), a schematic of which is shown in Fig. 1. The nozzle contains a vacuum window through which the proton beam enters the nozzle, a beam profile monitor to measure the shape and position of the beam, a beam reference monitor to measure the beam intensity, a scattering-power-compensated range-modulator wheel to modulate the penetration depth, a second scatterer to flatten the beam profile, a middle base plate that serves as an interface between the gantry and nozzle and as a shield to help prevent radiation leakage, a range

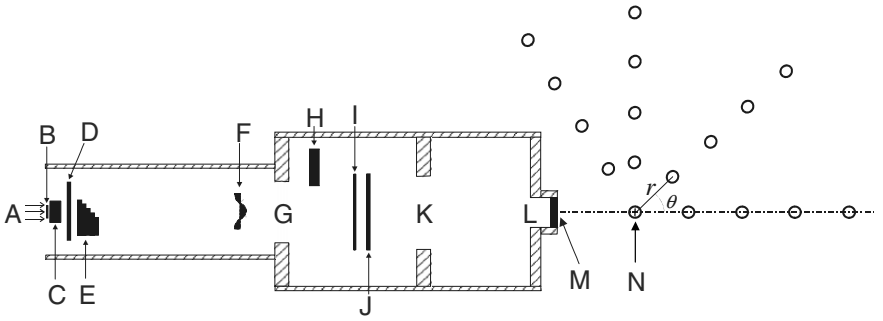

Fig. 1. Schematic of the passive scattering treatment nozzle used for the simulations. The model includes the proton source (A), a vacuum window (B), a beam profile monitor (C), a beam reference monitor (D), a scattering-power-compensated range-modulator wheel (E), a second scatterer (F), a mid base plate (G), a range shifter assembly (H), a backup monitor (I) a primary monitor (J), a pre-collimator (K), a snout (L), and an aperture (M). The isocenter is denoted by (N), and neutron receptors are denoted by open circles. r indicates the distance to isocenter and θ the angle with respect to the incident beam direction. Figure not to scale.

shifter assembly to adjust the beam range, primary and backup monitor chambers for beam termination, a pre-collimator to collimate the beam, and a snout that holds the final collimating aperture. Table 1 lists the materials from which these components are constructed and their locations in the nozzle.

The proton source was modeled with a mean energy of 250 MeV, an initial Gaussian energy profile ($\sigma_E = 0.42$ MeV), and a Gaussian lateral intensity profile ($\sigma_x = 2.3$ mm) located 328.5 cm from the isocenter (Fig. 1), the origin of our simulation coordination system. These parameters were taken from analytical beam optics calculations provided to us by the manufacturer.

To study the influence of the collimated field size on the neutron dose equivalent, the length of a side of the square final collimating aperture was varied from 0 to 18 cm in increments of 2 cm. The neutron spectral fluence (defined according to ICRU Report 60 [21]) was tallied in 12-cm-diameter spherical receptors located at isocenter and at distances of $r = 50$, 100, 150, and 200 cm from isocenter and at angles of $\theta = 0°$, 45°, 90°, and 120° with respect to the incident beam direction (see Fig. 1). In total, the neutron spectral fluence was tallied in receptors at 17 locations, including the isocenter. For each receptor, the neutron spectral fluence, $\Phi(E)$ (defined as $\frac{d\Phi}{dE}$), per proton entering the nozzle (p) was tallied in 438 logarithmically spaced bins from 10 meV to

Table 1
List of components, materials, and distance to isocenter for the major devices in the passive scattering proton therapy nozzle

Component	Material(s) of construction	Distance from isocenter (cm)
Vacuum window	Stainless steel	328.5
Beam profile monitor	Air filled, aluminum walls, tungsten wires	320.6
Reference monitor	Air-filled, copper-coated polyimide walls	317.1
Range-modulator wheel	Tungsten alloy and aluminum alloy	306.0
Second scatterer	Lead alloy and ABS resin	228.9
Mid base plate	Brass	210.0
Range shifter assembly	ABS resin	194.8
Backup dose monitor	Air filled, copper-coated polyimide walls	151.3
Primary dose monitor	Air filled, copper-coated polyimide walls	153.8
Pre-collimator	Brass	80.0
Snout	Brass	0–48.0 (20.0 in this work)
Aperture	Brass	20.0

1 GeV. Between 2×10^8 and 1×10^9 proton histories were simulated for each aperture size to ensure statistical uncertainties of less than 1% in the neutron fluence values and less than 5% for the neutron spectral fluence in the bins near 1 MeV neutron energy.

2.2. Calculations of neutron dose equivalent per therapeutic dose

The neutron dose equivalent is defined as the product of the neutron absorbed dose, D, and the mean quality factor, $\overline{Q}$. In this work, the neutron dose equivalent per proton was calculated as the product of the fluence per proton, $\Phi(E)/p$, and the fluence-to-dose-equivalent conversion coefficient, $h_\phi(E)$. The $h_\phi(E)$ values, which vary with the neutron energy, were taken from NCRP Report 38 [22], and the spectral fluence values per proton $\Phi(E)/p$ were obtained from the simulations, as described above. The neutron dose equivalent spectra per proton $H(E)/p$ was calculated using

$$H(E_i)/p = h_\phi(E_i) \cdot (\Phi(E_i)/p), \tag{1}$$

where E_i was the mean energy of the ith neutron energy bin. Performing a summation of the neutron spectral fluence over all energy bins, the neutron dose equivalent per proton (H/p) at each receptor location was given by

$$H/p = \sum_{i=1}^{n} (H(E_i)/p) \cdot E_i, \tag{2}$$

where n is the total number of energy bins and E_i is the energy width of the ith energy bin.

The therapeutic dose per proton (D/p) was, by definition, taken at the depth in a water phantom that corresponded to the maximum therapeutic absorbed dose from a pristine proton Bragg peak. The value of D/p was estimated from a separate simulation, using a geometry identical to that for H/p determinations except for the introduction of a phantom to stop the proton beam and omission of the neutron receptors. The phantom, a box of water measuring $40 \times 40 \times 40$ cm^3, was positioned with its upstream face normal to the incident beam and located at isocenter. The neutron dose equivalent per therapeutic dose in units of Sv Gy^{-1} was obtained using

$$\frac{H}{D} = \frac{H}{p} \Big/ \frac{D}{p}. \tag{3}$$

Using these methods, we investigated the influence of the therapeutic field size by calculating H/D values for 10 different aperture sizes and at three receptor locations. In addition, to examine the influence of the receptor location, we calculated H/D values at 17 locations. In the latter series of simulations, a closed aperture collimated the proton beam to zero field size.

2.3. Analytical modeling of H/D as a function of location

The behavior of $H(d)/D$ was presumed to be governed by a power-law relation to the distance d, or

$$H(d)/D = c \cdot d^{-\alpha}, \tag{4}$$

where c is a constant of proportionality, d is the effective source-to-receptor distance, and the exponent α is the main parameter that governs the shape of the falloff with distance. The effective source distance, d, was calculated using

$$d = \sqrt{(d_{\text{iso}} + r\cos\theta)^2 + r^2 \sin^2\theta}, \tag{5}$$

where d_{iso} was the effective neutron source-to-isocenter distance, and r and θ were as defined in Fig. 1. The parameters c, d_{iso}, and α were obtained from a multi-parameter conjugant gradient fit to the 17 $H(d)/D$ values obtained from simulations in which the final collimating aperture was closed, i.e., a 0×0 cm^2 field size.

3. Results

3.1. Distribution of dose equivalent in neutron energy

The energy-weighted neutron fluence and neutron dose equivalent spectra are plotted in Figs. 2 and 3, respectively. Three interaction mechanisms predominated in determining the shapes of these spectra. A low-energy peak, centered around 1 MeV, contained neutrons produced from evaporation processes. A high-energy peak, centered around 100 MeV, contained neutrons from direct (nucleon–nucleon) reactions from intranuclear cascades. Between these energies, neutrons ejected from compound-nucleus and pre-equilibrium processes were important. High-energy neutrons from the intranuclear cascade contributed about one-half to two-thirds of the neutron dose equivalent. Isotropically

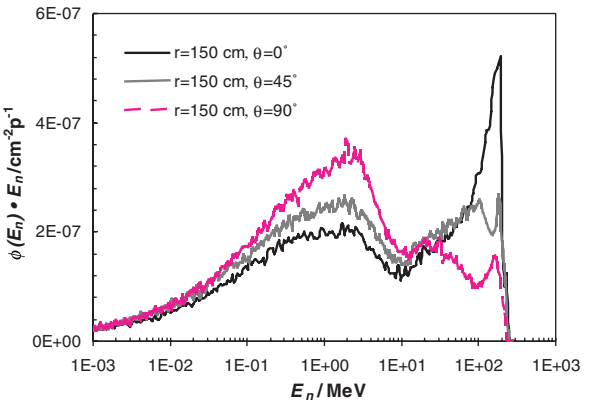

Fig. 2. Energy-weighted neutron fluence spectra ($\Phi(E_n) \cdot E_n$) as a function of neutron energy (E_n) around a passive scattering nozzle, with a 250-MeV beam entering the nozzle using a closed final proton collimating aperture. The spectra are from three locations: $r = 150$ cm and $\theta = 0°$; $r = 150$ cm and $\theta = 45°$; and $r = 150$ cm and $\theta = 90°$, where r is the distance from isocenter to the neutron receptor and θ is the angle between the beam axis and the vector from isocenter to the neutron receptor.

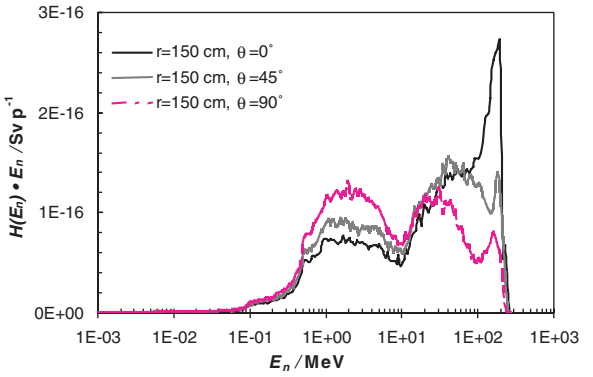

Fig. 3. Energy-weighted neutron dose equivalent spectra ($H(E_n) \cdot E_n$) as a function of neutron energy (E_n) around a passive scattering nozzle, with a 250-MeV beam entering the nozzle using a closed final proton collimating aperture. The spectra are from three locations: $r = 150$ cm and $\theta = 0°$; $r = 150$ cm and $\theta = 45°$; and $r = 150$ cm and $\theta = 90°$, where r is the distance from isocenter to the neutron receptor and θ is the angle between the beam axis and the vector from isocenter to the neutron receptor.

emitted low-energy neutrons from the evaporation process contributed about one-third to one-half of the total dose equivalent. Since the high-energy neutron component is forward peaked, it fell off rapidly as distance from the beam axis increased. This effect can be seen in Figs. 2 and 3, where the high-energy peak is the most prominent component along the beam axis ($r = 150$ cm, $\theta = 0°$) and the least prominent component lateral to the beam axis ($r = 150$ cm, $\theta = 90°$). Since the evaporation process is isotropic, the low-energy neutron component varies mainly with the nozzle-to-receptor distance. At a given isocenter-to-receptor distance (r), the nozzle-to-receptor distance decreases slightly as θ increases from 0° to 90°. This leads to a slight increase in magnitude in the low-energy peak at large angles, as shown in Figs. 2 and 3.

To estimate the uncertainties in H/D due to uncertainties in the shape of the neutron spectra, we examined variations in the mean neutron quality factors, $\overline{Q}$ as a function of location in the treatment room. We compared $\overline{Q}$ values from NCRP Report 38 [22] at the dose-equivalent-weighted mean neutron energy ($\overline{E}$) in each spectrum at each location considered in this work. The extrema of $\overline{E}$ were 43 MeV at isocenter and 21 MeV at $r = 150$ cm and $\theta = 120°$. Despite a factor-of-2 variation in $\overline{E}$, the corresponding $\overline{Q}$ values at these extrema (6.5 and 8, respectively) varied by less than 20%. The weak dependence of $\overline{Q}$ on $\overline{E}$ suggests that the uncertainties in H/D due to possible systematic errors in the shape of the neutron spectral fluences were negligible. The statistical uncertainties were less than 5% (one standard deviation) in any single energy bin of the neutron spectra in the energy interval between 1 and 200 MeV, which is responsible for approximately 90% of the total dose equivalent.

3.2. Influence of field size on neutron dose equivalent per therapeutic absorbed dose

To assess the influence of proton field size (FS) on neutron dose equivalent, we examined the ratio of $(H/D)_{FS}$ for each field size considered to the corresponding value obtained with a closed aperture, $(H/D)_0$ (i.e., a field size of zero). Fig. 4 plots $(H/D)_{FS}/(H/D)_0$ as a function of field size obtained at isocenter, at $r = 150$ cm and $\theta = 0°$ (150 cm downstream of isocenter), and at $r = 150$ cm and $\theta = 90°$ (150 cm laterally displaced from the central axis). When the aperture size was decreased from 18×18 to 10×10 cm^2, which is the interval of field sizes that would be used to deliver proton therapy to patients using the range modulator and second scatterer considered in this work, the neutron dose equivalent increased by approximately 29% at isocenter, 33% at $r = 150$ cm and $\theta = 0°$, and 9% at $r = 150$ cm and $\theta = 90°$.

The decrease in H/D with increasing field size can be understood in terms of the protons' eventual fate. As the collimating aperture size increased, a greater

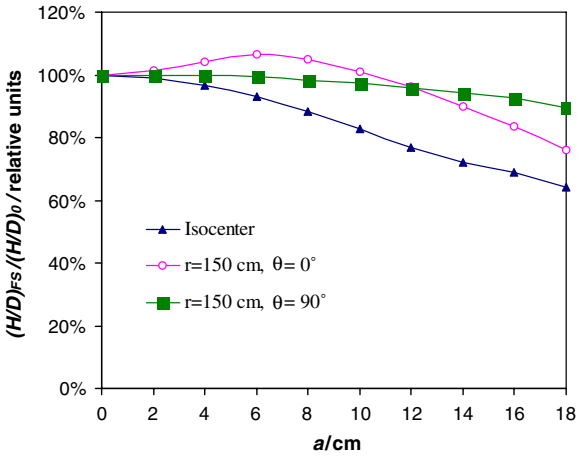

Fig. 4. Ratio of $(H/p)_{FS}$ to $(H/p)_0$ values for square fields as a function of the length (a) of the side of the square collimating aperture at isocenter (triangles), at $r = 150$ cm and $\theta = 0°$ (circles), and at $r = 150$ cm and $\theta = 90°$ (squares). The solid lines are visual guides from interpolations between these discontinuous data points.

fraction of the protons escaped from the nozzle without producing neutrons. One exception to this trend was at $r = 150$ cm and $\theta = 0°$, where the H/D values actually increased as the field size increased from 0×0 to 6×6 cm^2. This result can be explained by the fact that more neutrons generated from other components upstream of the nozzle, such as the range modulator, were allowed to enter the neutron receptor through the aperture when the aperture size was increased from 0×0 to 6×6 cm^2. The uncertainties in the H/D values are discussed in Section 3.3.

3.3. Influence of location on neutron dose equivalent per therapeutic absorbed dose

To obtain a conservative estimate of the $H(d)/D$ values as a function of position in the treatment room (d), we performed the simulations using a closed final collimating aperture. We adopted this approach because of our results (described in the previous section) demonstrating that the closed aperture yielded the highest $H(d)/D$ values in the vast majority of cases we considered.

The predicted values of $H(d)/D$ as a function of location around the nozzle are given in Table 2. The $H(d)/D$ value was largest at isocenter and decreased with increasing distance from isocenter for all angles considered. Given a constant distance to isocenter, the $H(d)/D$ values generally increased with increasing angle; notable exceptions to this

Table 2
Predicted neutron dose equivalent per therapeutic absorbed dose, H/D, as a function of angle with respect to the proton beam axis (θ) and distance from isocenter (r)

r (cm)	H/D (mSv Gy^{-1})			
	$\theta = 0°$	$\theta = 45°$	$\theta = 90°$	$\theta = 120°$
0	20.195	–	–	–
50	3.089	3.564	3.909	6.188
100	1.242	1.296	1.264	1.588
150	0.685	0.678	0.641	0.866
200	0.442	0.472	0.394	0.552

These values were obtained with a pristine 250-MeV proton beam entering the nozzle and a closed final collimator.

trend were the decreases in $H(d)/D$ as the angle increased from 45° to 90° at distances of 100, 150, and 200 cm.

Uncertainties in the simulated $H(d)/D$ values are believed to be large mainly because benchmark measurements are not available for the equipment considered in this work. Previous benchmark comparisons of simulations and measurements for the Harvard beamlines [7–10] revealed that the simulated values were systematically larger than the measured values. Part of this difference may be due to a systematic under-response of the instruments for neutrons with energies above 10 MeV [8], which contributed at least half the neutron dose equivalent in the present analysis (as discussed in Section 3.1). On the basis of these considerations, we estimated

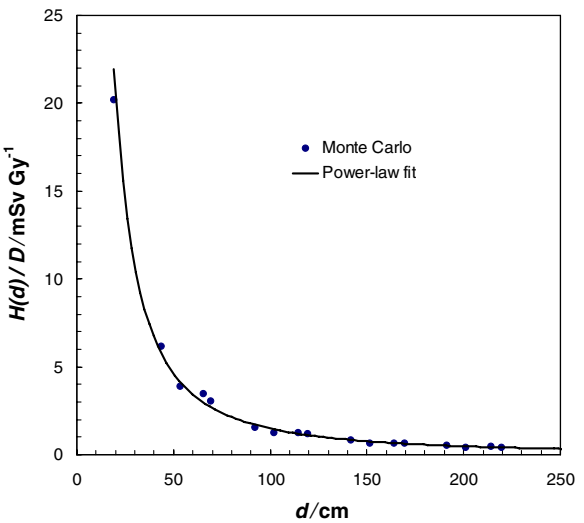

Fig. 5. The Monte Carlo and power-law predictions of the neutron dose equivalent, $H(d)$, versus d, the distance to the effective neutron source. These data correspond to a 250-MeV pristine proton beam blocked with a stopping-length final collimating aperture.

the uncertainty in our $H(d)/D$ values at about 40% (one standard deviation).

The power-law model accurately reproduced the relative $H(d)/D$ values at various locations in the treatment room. Fig. 5 plots the $H(d)/D$ values from the Monte Carlo simulations and from the power-law model predictions, revealing that agreement was within 9%, on average, and that the maximum discrepancy between the values was only 18%. These results are well within the uncertainties of the simulated $H(d)/D$ values. The values of the model parameters were $c = 2720$ mSv Gy^{-1}, $d_{iso} = 19.3$ cm (used to compute the d for each receptor using Eq. (5)), and $\alpha = 1.6$.

4. Discussion

The main findings of this study may be summarized as follows. First and most important, the neutron dose equivalent per therapeutic absorbed dose (H/D) generally decreased modestly as the collimated proton field size increased from zero (a fully blocked field) to 18×18 cm^2. Second, we found that it is possible to model $H(d)/D$ with a power-law relation in d, the distance to the effective neutron source. Third, an analysis of the distribution of neutron dose equivalent in neutron energy revealed that a substantial fraction (>50%) of the neutron dose equivalent was caused by neutrons with energies higher than 10 MeV. Our findings will allow us to take the next step toward routine prediction of H/D values in clinical treatment planning and may be helpful in designing future comparisons of $H(d)/D$ values from different types of proton therapy machines.

Our data are consistent with the maximum H/D value of 15 mSv Gy^{-1} reported by Yan et al. [7] for the Harvard passive scattering nozzle. Our findings on the power-law behavior of $H(d)/D$ with distance from the effective neutron source confirm and extend the modeling methods reported by Polf and Newhauser [8]. The $H(E_n)$ spectra from this work are qualitatively in good agreement with those from simulations by Polf and Newhauser [8] and in reasonable agreement with the measurements from Yan et al. [7]. The high-energy neutron component was less pronounced in the $H(E)$ measurements from Yan et al., because their instruments are believed to under-respond to high-energy neutrons. Like Yan et al. [7], we found that neutrons with energies of less than 10 keV (thermal and $1/e$ neutrons) do not contribute appreciably to the neutron dose equivalent because of the very small fluence-to-dose equivalent conversion coefficient in those energy regimes (about 3% of that for 1 MeV) as well as the relative low fluence in those regimes. As expected, the maximum H/D value from the present work was higher than the 5-mSv Gy^{-1} value reported by Schneider et al. [11] from a scanned-beam proton nozzle, which contains fewer materials in the beam path.

The results of this study, when applied to very small field sizes, should be interpreted with due consideration to the appropriateness of the scattering system used. In this study, H/p was determined in an 18×18 cm^2 proton beam, where it was implicitly assumed that the treatment field will ultimately be collimated to sizes in the interval between 10×10 cm^2 and 18×18 cm^2. To minimize neutron production, the machine at our institution was designed to produce three field sizes: small ($\leqslant 10 \times 10$ cm^2), medium (between 10×10 cm^2 and 18×18 cm^2), and large (between 18×18 cm^2 and 25×25 cm^2). To produce different collimated field sizes, the scattering system components (range-modulator wheel and second scattering foil) may be exchanged. (Although scattering components in our machine can be exchanged quickly and conveniently, many other machines do not have this capability.) It is clear that if one generates an uncollimated field size that is much larger than the final collimating aperture size, proton losses and neutron production in the aperture will be increased. Therefore, for our treatment machine, the results presented here for small field sizes are not an indicator of the minimum (lowest achievable) H/D values. In addition, in fields collimated to less than about 2 cm in diameter, the dose per proton decreases substantially because of a lack of lateral proton equilibrium in the patient or phantom [23]; this phenomenon is commonly called the field-size effect and would tend to increase H/D values. For these reasons, the reader is advised to interpret the H/D estimates from this work with due consideration to the uncollimated field size and the field-size effect.

Our study had several limitations. First, it was not possible for us to measure actual H/D values since the facility was still under construction at the time of the study. However, our Monte Carlo models were previously benchmarked against actual measurements [8–10] and so are believed to be reliable. Second, our study was limited to our institution's Hitachi proton therapy unit (ProBeaT);

however, similar findings are to be expected for similar machines, such as the treatment unit from ion beam applications [24]. Third, our results quantify only the neutron dose equivalent exposures associated with the beam delivery apparatus. The effects of the patient were intentionally excluded by determining the neutron spectral fluences free-in-air. Anatomical patient models (phantoms) have been shown to introduce complex neutron scattering and attenuation that cause H/D values to vary between patients and between various tumor locations within a patient [22]. Thus, we do not know how well the free-in-air H/D values from this study will predict the H/D values in anatomical phantoms. However, based on previous Monte Carlo studies [22], we believe the differences will be small in comparison with the associated uncertainties (cf. Refs. [7–10]).

The present results are important because they provide previously unavailable quantitative data on how the collimated field size affects H/D values. These data are potentially valuable in developing strategies to minimize the risk of late effects in patients receiving proton therapy. In particular, it is important to minimize the risk of second cancers in pediatric and young adult patients who have good prognoses. In addition, our study adds to the accumulating evidence suggesting that neutron dose equivalent exposures are non-negligible and warrant further study. Our findings suggest that the experimental approach used in this study (i.e., a closed-aperture condition and a free-in-air fluence determination) provides a simple and conservative means of estimating the exposures caused by neutrons produced within the treatment machine. However, the utility of this approach must be verified for a broader range of proton energies, modulation widths, and field sizes; these experiments are already under way in our laboratory.

5. Conclusions

We used Monte Carlo methods to estimate the neutron dose equivalent, H, caused by neutrons produced in a therapeutic proton beam delivery system; the therapeutic absorbed dose, D; and the distribution of dose equivalent in neutron energy, $H(E)$. Our findings revealed that H/D values in a contemporary proton therapy unit increased from 13 to 20 mSv Gy^{-1} at isocenter as the collimated proton field size was decreased from 18×18 to 0×0 cm^2. H/D values varied more strongly with location in the treatment room and generally decreased with distance to isocenter (20 mSv Gy^{-1} at isocenter, versus 0.9 mSv Gy^{-1} at 150 cm from isocenter). Neutron spectral fluence calculations revealed that >50% of the dose equivalent at all locations considered was from neutrons >10 MeV. Our results suggest that neutron exposures to patients who receive proton radiotherapy are small but not negligible and that further study is needed. The modeling methods developed here may be extended to ultimately provide H/D predictions in routine clinical treatment planning. In addition, our results suggest possible avenues for designing future investigations to compare $H(d)/D$ values from different therapy machines.

Acknowledgements

This work was supported by a research grant from Varian Medical Systems (Palo Alto, CA) and a faculty startup grant from The University of Texas MD Anderson Cancer Center to WN.

References

[1] A.M. Koehler, R.J. Schneider, J.M. Sisterson, Nucl. Instrum. and Meth. 131 (1975) 437.
[2] A.M. Koehler, R.J. Schneider, J.M. Sisterson, Med. Phys. 4 (1977) 297.
[3] B. Gottschalk, A.M. Koehler, J.M. Sisterson, M.S. Wagner, in: H. Blattmann (Ed.), Report 111, Proceedings of the Radiotherapy Workshop, held at the Paul Scherrer Institute, 29 February–1 March, 1991, P.S.I., Villigen, Switzerland, 1991, p. 50.
[4] J. Sisterson, Nucl. Instrum. and Meth. B 241 (2005) 713.
[5] P.J. Binns, J.H. Hough, Radiat. Prot. Dosim. 70 (1997) 441.
[6] S. Agosteo, C. Birattari, C. Caraviggio, M. Silari, G. Tosi, Radiother. Oncol. 48 (1998) 293.
[7] X. Yan, U. Titt, A. Koehler, W. Newhauser, Nucl. Instrum. and Meth. A 476 (2002) 429.
[8] J.C. Polf, W.D. Newhauser, Phys. Med. Biol. 50 (2005) 3859.
[9] J.C. Polf, W.D. Newhauser, U. Titt, Radiat. Prot. Dosim. 115 (2005) 154.
[10] J.D. Fontenot, W.D. Newhauser, U. Titt, Radiat. Prot. Dosim. 116 (2005) 211.
[11] U. Schneider, S. Agosteo, E. Pedroni, J. Besserer, D. Phys, Int. J. Radiat. Oncol. Biol. Phys. 54 (2002) 244.
[12] S.C. Roy, G.A. Sandison, Radiat. Phys. Chem. 71 (2004) 997.
[13] H. Jiang, B. Wang, X. Xu, H. Suit, H. Paganetti, Phys. Med. Biol. 50 (2005) 4337.
[14] D. Pelowiz (Ed.), MCNPX User's Manual version 2.5.0 LA-CP-05-0369, Los Alamos National Laboratory, Los Alamos, NM, 2005.
[15] J. Hérault, N. Iborra, Med. Phys. 32 (2005) 910.
[16] M.B. Chadwick, P.G. Young, S. Chiba, S.C. Frankle, G.M. Hale, H.G. Hughes, A.J. Koning, R.C. Little, R.E.

MacFarlane, R.E. Prael, L.S. Waters, Nucl. Sci. Eng. 131 (1999) 293.
[17] H.W. Bertini, Phys. Rev. 188 (1968) 1711.
[18] Y. Yariv, Z. Fraenkel, Phys. Rev. 20 (1979) 2227.
[19] Y. Zheng, W.D. Newhauser, J.D. Fontenot, N.C. Koch, in: Proceedings of the American Nuclear Society 14th Biennial Topical Meeting of the Radiation Protection and Shielding Division, held 3–6 April 2006, American Nuclear Society, Carlsbad, NM, 2006, p. 256.
[20] W. Newhauser, J. Fontenot, Y. Zheng, J. Polf, U. Titt, N. Koch, R. Mohan, Phys. Med. Biol., submitted for publication.
[21] International Commission on Radiation Units and Measurements (ICRU), ICRU Report Number 60, ICRU, Bethesda, MD, 1998.
[22] National Council on Radiation Protection and Measurements (NCRP), NCRP Report 38, NCRP, Bethesda, MD, 1971.
[23] A. Koehler, W. Preston, unpublished manuscript, Cambridge, MA, Harvard Cyclotron Laboratory, 1967.
[24] Y. Jongen, W. Beeckman, P. Cohilis, Bull. Cancer/Radiother. 83 (1996) 219s.